Influence of Pluronic F68 on Size Stability and Acoustic Behavior of Monodisperse Phospholipid-Coated Microbubbles Produced at Room Temperature

Wang, Yuchen; Spiekhout, Sander; Walgode, Ana; Collado-Lara, Gonzalo; van der Steen, Antonius F.W.; de Jong, Nico; Bosch, Johannes G.; Johnson, Benjamin R.G.; Kooiman, Klazina

DOI
10.1021/acsami.4c18844

Publication date
2025

Document Version
Final published version

Published in
ACS Applied Materials and Interfaces

ACS APPLIED MATERIALS & INTERFACES

www.acsami.org
Research Article

Influence of Pluronic F68 on Size Stability and Acoustic Behavior of Monodisperse Phospholipid-Coated Microbubbles Produced at Room Temperature

Yuchen Wang,* Sander Spiekhout, Ana Walgode, Gonzalo Collado-Lara, Antonius F. W. van der Steen, Nico de Jong, Johannes G. Bosch, Benjamin R. G. Johnson, and Klazina Kooiman

Cite This: ACS Appl. Mater. Interfaces 2025, 17, 8976−8986
Read Online

ACCESS | Metrics & More | Article Recommendations | Supporting Information

ABSTRACT: Ultrasound contrast agents, comprised of phospholipid-coated microbubbles, can be produced as monodisperse populations using a microfluidic flow-focusing device. However, microbubble coalescence remains a significant challenge. High production temperatures (e.g., 55 °C) can be used to suppress coalescence, but it complicates the microfluidic device design and is incompatible with targeting agents and drug conjugates. This study investigates the production of monodisperse microbubbles at room temperature with the addition of the amphiphilic surfactant Pluronic F68. Two 1,2-distearoyl-*sn*-glycero-3-phosphocholine (DSPC)-based phospholipid formulations were investigated: F1, containing 1,2-dipalmitoyl-*sn*-glycero-3-phosphoethanolamine-*N*-[carbonyl-methoxypolyethylene glycol] (DPPE-PEG5000), and F2, which included both DPPE-PEG5000 and polyoxyethylene(40) stearate (PEG40-stearate). We characterized the size stability and acoustic behavior of monodisperse microbubbles produced with various Pluronic F68 concentrations. Adding 5−10 mol % Pluronic F68 was found to effectively suppress coalescence and facilitated the production of monodisperse microbubbles that remained shelf stable for at least 7 days. Acoustic attenuation measurements revealed a shell stiffness ranging from 0.78 to 0.93 N/m for these microbubbles. The 10 mol % Pluronic F68 addition (10PF) demonstrated superior monodispersity and was selected for further experiments. Upon dilution, the size and resonance frequencies of both F1−10PF and F2−10PF decreased over time, though F2−10PF showed better stability compared to F1−10PF for both metrics. Both F1−10PF and F2−10PF exhibited a stronger subharmonic scattering intensity than SonoVue (clinical approved microbubbles), which offers potential for blood pressure sensing. Our study shows that incorporating Pluronic F68 facilitates the production of monodisperse microbubbles at room temperature that are stable long-term and have excellent acoustical properties, with the F2−10PF formulation demonstrating better stability than the F1−10PF.

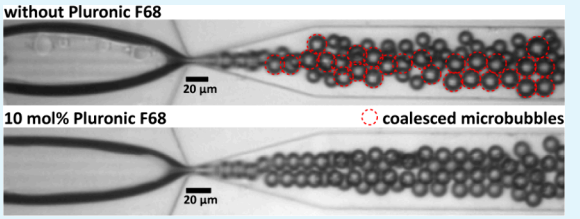

KEYWORDS: *ultrasound contrast agents, phospholipid coating, monodisperse microbubbles, Pluronic F68, stability, shell elasticity, subharmonic, resonance behavior*

INTRODUCTION

Ultrasound contrast agents, comprising of gas microbubbles ranging from 0.5 to 5 μm in radius, play an important role in clinical echography and therapy.[1,2] Administered intravenously, microbubbles circulate in the bloodstream through the entire vascular tree, acting as blood pool agents due to their size that prevents diffusion through the endothelium.[3,4] The lifetime of these microbubbles is prolonged by a phospholipid coating that minimizes Laplace pressure driven diffusion.[5,6] When subjected to ultrasound, these microbubbles start to oscillate thereby generating echoes due to the high compressibility of the gas core.[7,8] The scattering of microbubbles is strongest at resonance, which depends on the microbubble radius, acoustic driving pressure, and mechanical properties of the shell. The resonance frequency of a microbubble is inversely proportional to its radius, i.e., a smaller microbubble has a higher resonance frequency and vice versa.[9] Clinically approved ultrasound contrast agents have a wide size distribution, resulting in a broad range of resonance frequencies.[10−12] As clinical ultrasound probes typically operate in a relative narrow frequency bandwidth,[13] only a fraction of the microbubble population oscillates effectively. Utilizing microbubbles with a narrow size distribution (i.e., monodisperse) has been shown to increase the intensity of contrast enhanced ultrasound imaging by 2 to 3 orders of magnitude.[14] Furthermore, monodisperse microbubbles have shown to improve the drug delivery efficiency by nearly 1 order of magnitude,[15] and

Received: October 30, 2024
Revised: December 13, 2024
Accepted: December 16, 2024
Published: February 3, 2025

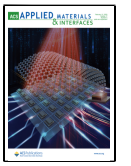

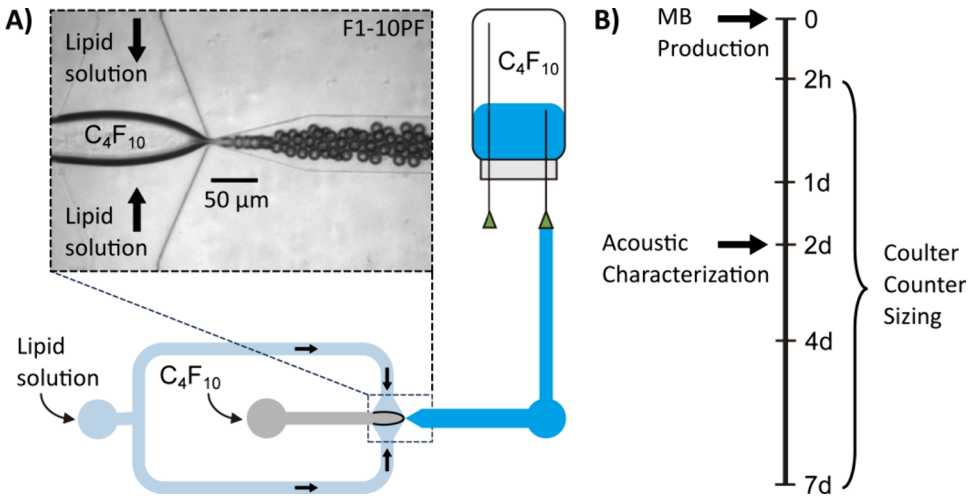

Figure 1. Microbubble production setup and characterization timeline. (A) Schematic illustration of the flow-focusing microfluidic chip for monodisperse microbubble production (not drawn to scale). The lipid solution and C_4F_{10} gas are pumped into the system, and the produced microbubbles are collected in a gastight vial prefilled with C_4F_{10} in the headspace. The inset shows a high-speed image of microbubbles forming at the nozzle for phospholipid formulation F1 with 10 mol % Pluronic F68 addition (F1−10PF). (B) Timeline for the microbubble size distribution measurements and acoustic characterization following microbubble production.

double the sensitivity of pressure sensing via the subharmonic microbubble signal.[16,17] Therefore, producing microbubbles with a monodisperse size and uniform acoustic response is crucial to unlock the full potential of microbubbles for ultrasound (molecular) imaging as well as for therapy.

Monodisperse microbubbles can be produced directly using a microfluidic flow-focusing chip. In such a device, a gas thread is focused between two aqueous liposome flows,[18,19] resulting in a shear stress along the gas−liquid interface that facilitates the opening and fusion of liposomes onto the interface.[20] This process enables the gas thread to pinch-off reproducibly, thereby allowing for high-speed production (typically in the range of 10^4−10^6 microbubbles per second) of monodisperse microbubbles.[21,22] These freshly formed microbubbles have a loosely packed phospholipid coating[23] and are inherently unstable, leading to a gradual decrease in size until they reach a stable final size. This stabilization process also results in a foam bubble layer due to Ostwald ripening.[21,24] Moreover, a major challenge for the production of monodisperse microbubbles is coalescence, where two or more microbubbles merge into one bigger microbubble. An elevated temperature during production has been shown to suppress coalescence.[25] Yet, elevated temperatures complicate the design of the microfluidic system and may not be compatible with targeting agents and/or potential drug-conjugates.[26] Hence, the use of additional surfactants, such as polymers or nanoparticles, could provide an promising alternative strategy to suppress coalescence.[24]

The synthetic amphiphilic copolymer Pluronic F68 ($(PEO)_{78}$-$(PPO)_{30}$-$(PEO)_{78}$), also known as Poloxamer 188, is FDA approved as a therapeutic reagent to reduce blood viscosity in the blood before transfusions.[27,28] Adding 94.7 mol % Pluronic F68 has been reported to effectively suppress coalescence in the production of protein-shelled monodisperse microbubbles with a shelf-stability up to 7 d.[29−31] Coalescence was also effectively suppressed when 87.7 mol % Pluronic F68 was added during the production of phospholipid-shelled monodisperse microbubbles, specifically with a DSPC-based coating.[32] However, the stability measurement was limited to 10 min postproduction, which is much shorter than the approximately 2 h stabilization process needed for phospholipid-shelled monodisperse microbubbles.[21,33] Adding a surfactant can influence the shell structure,[34] potentially affecting the uniformity of echo responses,[23,34] including the subharmonic response.[17] Pluronic F68 was shown to be able to tune the mechanical properties of a protein-based monodisperse microbubble formulation.[35] However, the effect of Pluronic F68 on the acoustic behavior of phospholipid-shelled monodisperse microbubbles remains to be studied.

This study investigates the effects of varying Pluronic F68 molar concentrations on phospholipid-shelled monodisperse microbubbles produced by a flow-focusing method at room temperature. Two DSPC-based phospholipid shell formulations were investigated: one binary mixture with 1,2-dipalmitoyl-*sn*-glycero-3-phosphoethanolamine-N-[carbonyl-methoxypolyethylene glycol] (DPPE-PEG5000) and one ternary mixture with DPPE-PEG5000 and polyoxyethylene(40) stearate (PEG40-stearate). To determine the microbubble stabilization process and shelf stability, the microbubble size distribution was measured from on-chip to 7 d postproduction. The stability of the microbubbles upon dilution in saline solution was measured over time. The microbubble shell properties were inferred from bulk acoustical attenuation measurements. Bulk scattering measurements were performed to quantify the (sub)harmonic content of the microbubble signal and the uniformity in the acoustical response of single microbubbles was determined from acoustical camera measurements.

MATERIALS AND METHODS

Materials. The lipids DSPC and DPPE-PEG5000 were kindly provided by Lipoid GmbH (Ludwigshafen, Germany). PEG40-stearate was purchased from Sigma-Aldrich (Zwijndrecht, The Netherlands). Pluronic F68 was purchased from Thermo Fisher Scientific (Waltham, Massachusetts, USA). Perfluorobutane (C_4F_{10}) was purchased from F2 Chemicals (Preston, UK), and argon gas was purchased from Linde Gas Benelux (Schiedam, The Netherlands).

Phospholipid Formulations. Two lipid formulations were investigated in this study. The first formulation (F1) was a binary mixture of DSPC and DPPE-PEG5000 in a molar ratio of 90:10 as previously reported by others.[33] The second formulation (F2) was a ternary mixture of DSPC, DPPE-PEG5000, and PEG40-stearate in a

https://doi.org/10.1021/acsami.4c18844
ACS Appl. Mater. Interfaces 2025, 17, 8976−8986

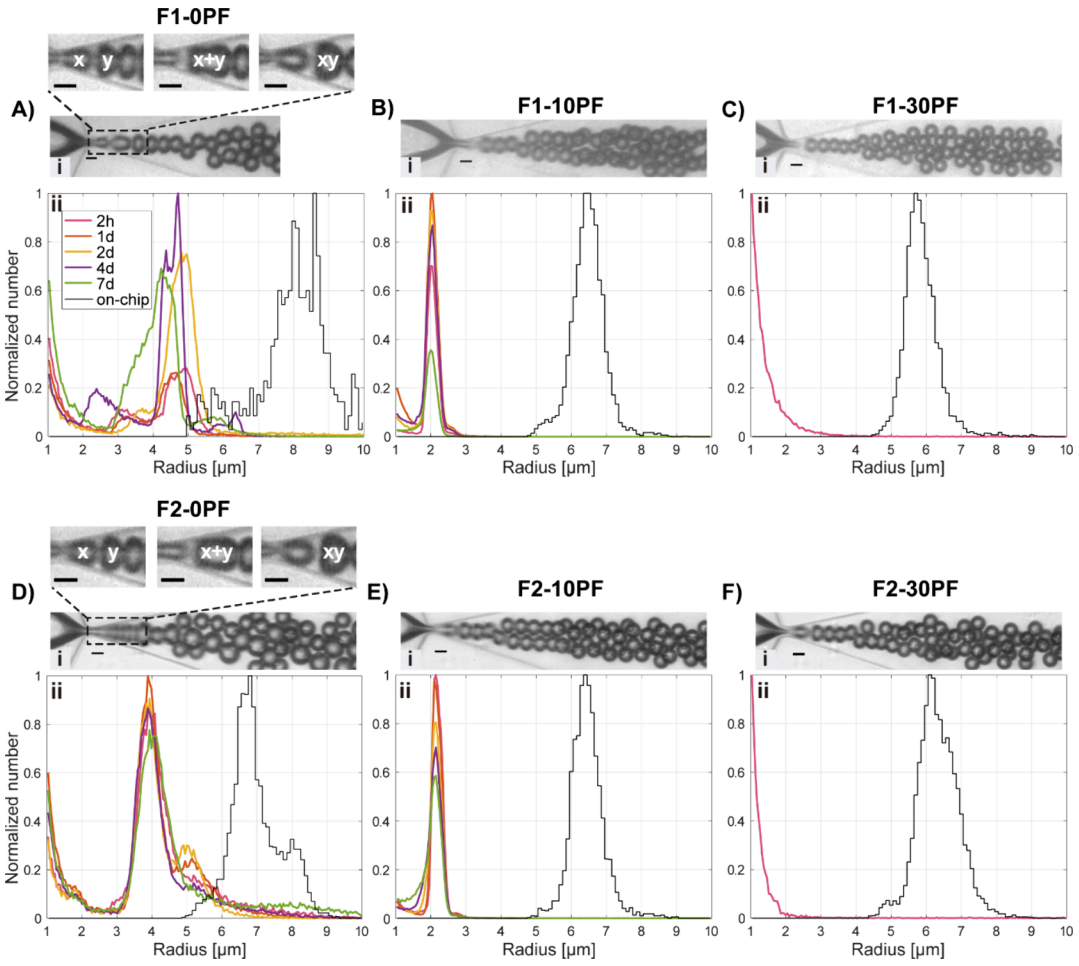

Figure 2. Monodisperse microbubble production and shelf stability. (i) Selected frames of the high-speed imaging of microbubble formation right after pinch-off. The insets of (Ai) and (Di) are a zoom in of the dashed rectangles in (i); "x" and "y" indicates individual microbubbles that form a larger coalescence microbubble "x+y". (ii) Normalized number-weighted size distributions measured on-chip (black) and postproduction (colors). (A) F1−0PF. (B) F1−10PF. (C) F1−30PF. (D) F2−0PF. (E) F2−10PF. (F) F2−30PF. All scale bars represent 10 μm.

molar ratio of 82.1:10:7.9. The lipids were prepared with the previously described indirect method.[34] Briefly, lipids were mixed and dissolved in chloroform/methanol (90:10 v/v %). The mixture was then evaporated under argon gas and the obtained lipid film was freeze-dried (Alpha 1−2 LD plus; Mertin Christ GmbH, Osterode am Harz, Germany) under vacuum overnight. The lipid film was then rehydrated in PBS at 55 °C to achieve a total lipid concentration of 20 mg/mL, followed by incubation in a 55 °C water bath for 40 min with vortexing every 15 min. Subsequently, Pluronic F68 was added to the mixture to reach molar percentages of 0 (0PF), 5 (5PF), 7.2 (7.2PF), 10 (10PF) and 30 (30PF) while maintaining the original lipid molar ratio. Finally, the mixture was placed into a sonication bath at 55 °C for 20 min. The obtained solution was then put on the bench to cool down to room temperature.

Flow-Focusing Chip Fabrication. The master mold for fabricating the flow-focusing chips was created as previously described.[36] Detailed methods for fabricating the flow-focusing microfluidic chip are provided in Supporting Information. The resulting flow focusing chip featured a uniform depth of 24.5 μm and a 5 μm wide nozzle that expanded to a 60 μm wide outlet channel (Figure 1A).

Microbubble Production and Collection. Microbubbles were produced at room temperature using the Horizon microfluidic platform.[36] A high-speed-camera (NOVA S16, Photron, Japan) was used to monitor the production process at a frame rate of 200 (Figure 2i) or 600 kfps (inset of Figure 2Ai,Di). An external high-intensity LED light source (MultiLed QT, GS02370, Germany) was used to illuminate the chip during high-speed imaging. Throughout microbubble production, the C_4F_{10} gas pressure was maintained at 800 mbar while adjusting the flow rate of the lipid solution to achieve a mean on-chip microbubble radius of approximately 6 μm. The on-chip size distribution was measured from these high-speed imaging using a custom MATLAB script (The Mathworks Inc., Natick, MA, USA), from which the mean initial on-chip radius (R_i) was derived using a Gaussian fit. As shown in Figure 1A, the outlet of the chip was connected to a 19G needle that was pierced through the rubber stopper of an inverted collecting glass vial (Z113964−288EA, Sigma-Aldrich, Zwijndrecht, The Netherlands) pre-filled with C_4F_{10} in the head space. A venting needle was inserted into the collecting vial during the microbubble production. After completing the collection, both needles were removed, and the vial was positioned upright, the monodisperse microbubbles were stored at room temperature.

Microbubble Stability. The shelf stability of the produced microbubbles was assessed by measuring the size distribution and concentration at 2 h, 1 d, 2 d, 4 d, and 7 d postproduction (Figure 1B) using a Coulter Counter Multisizer 3 (50 μm aperture tube; Beckman Coulter, Mijdrecht, The Netherlands) by diluting 10 μL microbubble suspension in 20 mL Isotone-II (Beckman Coulter) at room temperature and waiting 3 min before measuring. The microbubble concentration of each microbubble type was normalized to the highest concentration observed during the 7-day period. Monodispersity of the microbubble samples was assessed by calculating the coefficient of variation (CoV = $(\sigma/\mu) \times 100\%$), where μ is the mean microbubble size and σ the standard deviation. The μ and σ were determined by fitting a Gaussian through the Coulter Counter data using the above-mentioned custom-developed

https://doi.org/10.1021/acsami.4c18844
ACS Appl. Mater. Interfaces 2025, 17, 8976−8986

MATLAB script. Additionally, the ratio of the mean initial on-chip radius (R_i) to the final stable radius (R_f) was determined for each microbubble type, where R_f is the mean (μ) value obtained from the size distribution 2 d postproduction.

The stability of microbubbles upon dilution was evaluated using the Coulter Counter Multisizer 3 over a 30 min period, with Isotone-II as the diluent. A 10 μL microbubble suspension was diluted in 100 mL Isotone-II at room temperature. Size distribution and concentration changes were measured for a period of 30 min with data recorded at 2.5 min intervals. A stirrer ensured homogeneous distribution of the microbubbles in the dilution during the measurements.

Acoustic Characterization. All acoustic characterization measurements were performed 2 d postproduction (Figure 1B). This time point was chosen to allow sufficient time for the microbubbles to stabilize in the vial and has previously been used by others.[37]

Attenuation Measurements. For the attenuation experiments, microbubble suspensions were prepared by diluting 2 μL of the microbubble liquid from the collection vial in 100 mL of Isotone-II and waiting at least 2 min. Thirty mL of the diluted microbubble suspension was then added to a rectangular bubble container (24 × 24 × 55 mm; W × D × H) which had acoustic windows (13 × 38 mm; W × H) made from a thin (250 μm) polyester sheet to minimize acoustic diffraction. Inside this container, the microbubble suspension was kept homogeneous by continuously stirring with a magnetic stirrer. The microbubbles were then subjected to 12-cycle pulses in the frequency range of 1 to 5 MHz in 100 kHz increment intervals with peak negative pressure amplitudes of 10, 25, 75, and 150 kPa (41 × 4 pulses) using a programmable waveform generator (WW2572A, 250 MS/s, Tabor Electronics, Nesher, Israel), amplifier (310L, ENI, Rochester, NY, USA) and transmitting transducer (PA081, Precision Acoustics, Dorchester, UK). The individual pulses were Tukey tapered over the first and last two cycles and separated by a 300 μs rest period. The acoustic pressures were calibrated with a needle hydrophone (1 mm diameter, PA2293, Precision Acoustics) in a separate measurement. The acoustical signal was received by a receiving transducer (PA275, Precision Acoustics) and digitized (M4x.4420-x4, Spectrum Instrumentation, Limerick, Ireland) without amplification and stored on a computer. The entire sequence was recorded ten times with a 5 s interval to avoid repeated insonifications and to allow averaging. Three attenuation measurements were performed on a fresh diluted microbubble suspension for each microbubble sample. A measurement on an Isotone-II solution without microbubbles was captured as reference. Attenuation spectra were obtained by dividing the received magnitude of the individual pulses by the reference measurement and averaging over the 10 measurements. The recorded attenuation spectra at 10 kPa and Coulter Counter data were then used to fit to a Rayleigh-Plesset model to obtain the shell elasticity and shell viscosity.[37] The measured attenuation spectra were normalized to a concentration of 5.5×10^4 microbubbles/mL,[37] to account for the variance in concentration and total volume of the various microbubble formulations.

Scattering Measurements. The scattering of the microbubbles was measured in a separate acoustical experiment. The microbubbles were diluted in a 6.5 × 6.5 cm PMMA container, with thin (20 μm thick) polyester acoustic windows in the ultrasound beam path to minimize diffraction. The container was placed in a water tank, within the focus of a single element transducer (V381, 3.5 MHz, 0.75 in. diameter, 3 in. focus, Olympus, Tokyo, Japan) that was used to transmit a sequence of acoustic pulses. The sequence, generated by an arbitrary waveform generator (AWG, WW257la, Tabor Electronics), consisted of multiple 30-cycles acoustic pulses, where the first and last five cycles were apodized, with increasing frequencies, from 2.5 to 4.5 MHz in 500 kHz increments, and increasing peak negative amplitudes, from 250 to 550 kPa in 50 kPa increments (100 kPa increment for SonoVue) (35 sequences in total). The sequence was repeated 32 times for averaging purposes. The acoustic pressure was calibrated in a separate measurement with a 0.2 mm needle hydrophone (Precision Acoustics). The scattered microbubble signal was received by an unfocused single element transducer (V309, 5 MHz, 0.5 in. diameter), aimed toward the PMMA tank, amplified 58 dB (Miteq AU1519, Hauppauge, NY, USA), and recorded with an oscilloscope (PicoScope 5443D, Pico Technology, Cambridgeshire, UK) at 125 MHz sampling frequency and 15 bits resolution.

The monodisperse microbubbles used for the scattering measurements, F1−10PF and F2−10PF, were produced in a different batch from those used in the attenuation measurements. SonoVue (Bracco, Plan-LesOuates, Switzerland) was measured as a reference, which was activated on the same day of the experiments. The dilution was adapted for each formulation to provide an approximate attenuation of 2 dB/cm (1 μL of monodisperse microbubbles and 20 μL of SonoVue diluted in 130 mL of Isoton- II). The suspension was added to the scattering tank where it was continuously stirred and left to rest for 2.5 min before acquisition. The received signals were analyzed using MATLAB. The magnitude of the frequency spectrum, obtained with the fast Fourier transform, was averaged among the 32 acquisitions and log compressed.

Acoustical Camera. The resonance curve of individual monodisperse microbubbles was obtained by using high-frequency geometrical scattering in an "acoustical camera" setup[38] as previously described.[23] Briefly, single microbubbles were driven into oscillation by an acoustic pulse with a linearly increasing frequency (chirp) in the range of 1 to 5 MHz over 50 μs with pressures of 7, 14, 28, and 42 kPa. Simultaneously, a 25 MHz probing pulse was transmitted to the vibrating microbubble, and the perpendicularly scattered high-frequency signal was received. Since the scattered high-frequency signal is modulated as a function of the varying microbubble radius (oscillation induced by the lower-frequency pulse), the radial dynamics of the microbubble can be extracted.[38] For both F1−10PF and F2−10PF microbubbles, three acoustical camera measurements were performed for 20 min each. In total 659 (F1−10PF) and 562 (F2−10PF) resonance curves of single microbubbles were obtained after preselecting signals as described previously.[23] The resonance frequencies f_{res} in response to the 7 kPa pulse were then extracted and plotted as a function of the time t since the start of the measurement. To quantify the change in the observed resonance frequencies over time, an exponential function $f = a \times \exp(-b \times t)$ was fitted through the $f_{res}(t)$ results to obtain the moving average. Additionally, to obtain the variability, the standard deviation of the moving average was determined.

RESULTS AND DISCUSSION

Microbubble Production. The influence of Pluronic F68 on the production of monodisperse microbubbles was investigated for the two phospholipid formulations F1 and F2 and five different Pluronic F68 mol %. In the absence of Pluronic F68, immediate microbubble coalescence was observed for both formulations upon microbubble pinch off from the gas thread (Figure 2Ai,Di). Notably, F1−0PF generated a monodisperse population of microbubbles, resulting from the consistent coalescence of two microbubbles. Despite this on-chip uniformity, F1−0PF was unstable over a 7-d period in the collecting vial (Figure 2Aii). In line with our observation, a previous study indicated that a formulation without Pluronic F68, consisting of DSPC, DPPA, and DPPE-PEG5000, resulted in 70% of the microbubbles to coalescence at room temperature.[25] By contrast, the F2−0PF showed a characteristic secondary peak with a radius at $\sqrt[3]{2}$ times the first peak radius, indicating only part of the microbubble population coalesced on chip.

The addition of 5PF, 7.2PF, 10PF, and 30PF effectively suppressed on-chip coalescence for both formulations (Figures 2B,C,E,F and S1). Postproduction, a temporary increase in microbubble concentration was observed, peaking at 2 d for F1−5PF, F1−7.2PF, F1−10PF, and F2−5PF, and at 1 d for F2−7.2PF, followed by a decrease until 7 d. In contrast, the

https://doi.org/10.1021/acsami.4c18844
ACS Appl. Mater. Interfaces 2025, 17, 8976−8986

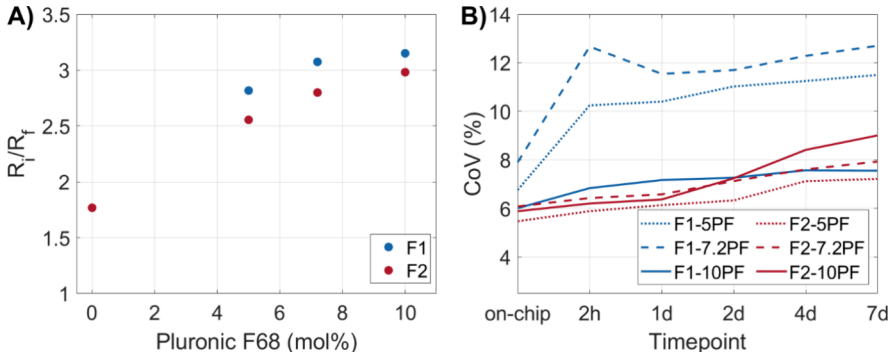

Figure 3. Quantification of R_i/R_f and monodispersity. (A) R_i/R_f ratio for both formulations with increasing Pluronic F68 from 0 to 10 mol %. (B) Coefficient of variation (CoV = $(\sigma/\mu) \times 100\%$) of size distribution from on-chip production to 7 d postproduction for both formulations with 5 to 10 mol % Pluronic F68 addition.

F2−10PF displayed a continuous decrease in concentration from 2 h to 7 d. During storage, two simultaneous processes occur: the shrinkage of foam bubbles formed through Ostwald-ripening[39] into a stable monodisperse size, potentially increasing the microbubble concentration,[21,33] and the concurrent collapse of microbubbles, which lowers the concentration.[33] Therefore, the measured concentration represents the net effect of these two simultaneous processes. These foam bubble can be minimized by mixing a high-aqueous-solubility gas, such as CO_2, into the C_4F_{10} gas core during production.[33] However, this strategy cannot be readily implemented with the Horizon system. By contrast, 30PF (Figure 2C,F) addition suppressed the coalescence during production but produced microbubbles did not stabilize to a monodisperse microbubble population within 2 h postproduction. Consequently, F1−30PF and F2−30PF microbubbles were not further investigated. While it has been shown that the addition of 87.7 mol % Pluronic F68 can produce monodisperse microbubbles with a DSPC-based formulation,[32] these microbubbles were monitored for only 10 min postproduction. Other studies have indicated that it could take more than 2 h for microfluidic-formed monodisperse microbubbles to stabilize to their final size.[25,40] Therefore, it remains unclear whether the addition of 87.7 mol % Pluronic F68 would have resulted in a stabilized monodisperse microbubble population after 2 h.

To assess the influence of Pluronic on the microbubble stabilization process, R_i/R_f was plotted as a function of Pluronic F68 mol % in Figure 3A. For the F1−0PF, we could not calculate the ratio R_i/R_f due to the severe on-chip coalescence. For the same lipid formulation as F1−0PF produced at a higher temperature, a R_i/R_f ratio of 2.2 has been reported,[33] which is higher than the ratio of 1.8 of F2−0PF. For both formulations, the R_i/R_f shows an increasing trend from 5PF to 10PF addition. This finding aligns with previously reported findings where the R_i/R_f increases with surfactant DPPE-PEG5000 and propylene glycol addition.[24] In our study, F1 demonstrated a higher R_i/R_f than F2 within the 5PF to 10PF range. This aligns with our previous finding that the ternary mixture (DSPC: DSPE-PEG2000: PEG40-stearate) had a higher area per lipid molecule than the binary mixture (DSPC: DSPE-PEG2000) up to a surface pressure of around 28 mN/m, as measured by a Langmuir trough at 20 °C.[41] Moreover, the absence of a squeeze-out plateau in that Langmuir trough curve during monolayer compression may suggest that PEG40-stearate retention in the shell results in the lower R_i/R_f observed for F2 microbubbles. It has been suggested that the retention of PEG40-stearate in the microbubble's lipid shell results from attractive, short-range dispersion forces from the hydrophobic acyl chains of the adjacent lipids, which anchor PEG40-stearate into the shell.[42] The highest ratio R_i/R_f of 3.2 for F1−10PF and 3.0 for F2−10PF are slightly above the highest reported ratio of 2.8 for similar formulations.[24]

To assess the monodispersity from on-chip production to 7 d postproduction, the CoV was quantified for each microbubble sample, as shown in Figure 3B. The microbubbles remained monodisperse during storage with a 1.7−4.8% increase in CoV over 7 d, with F2 demonstrating a lower CoV than F1 at all Pluronic F68 additions. The mean microbubble radius for all our samples remained stable, decreasing less than 4% over the 7 d (Figure S2A). This radius decrease is notably less than the rapid 10% radius decrease within 1 d post production reported for DSPC-based monodisperse microbubbles,[16] and the 10% radius reduction observed in protein-shelled monodisperse microbubbles over 7 d.[31] In terms of monodispersity, previous studies have shown that polymer-coated monodisperse microbubbles can achieve a CoV of 5.5% directly after production, close to the 6% CoV observed in our on-chip microbubbles.[43] Our results demonstrated a gradual increase in CoV over time, consistent with other studies on monodisperse phospholipid microbubbles.[21,25] This suggests that early use of monodisperse microbubbles postproduction would yield the best results for clinical applications.

The increase of R_i/R_f with increasing Pluronic F68 molar percentage may suggest that more Pluronic F68 is expelled from the microbubble coating at higher molar percentages. From Langmuir trough experiments, it is known that Pluronic F68 is fully expelled from dipalmitoylphosphatidylcholine (DPPC) monolayers at surface pressures higher than 26 mN/m at room temperature, below which Pluronic F68 remains in the monolayer.[44,45] We speculate this happened in our system. During microbubble production, freshly formed monodisperse microbubbles are inherently unstable and always shrink in size,[21,40] which increases the surface pressure of the shell, thus potentially allowing Pluronic F68 to expel from the coating. Therefore, we attribute the increase in R_i/R_f with higher Pluronic F68 concentrations to the expelling of greater amounts of Pluronic F68 from the shell. Strategically adjusting Pluronic F68 levels to achieve higher R_i/R_f could allow a wider nozzle to produce the smaller microbubbles, which could allow

https://doi.org/10.1021/acsami.4c18844
ACS Appl. Mater. Interfaces 2025, 17, 8976−8986

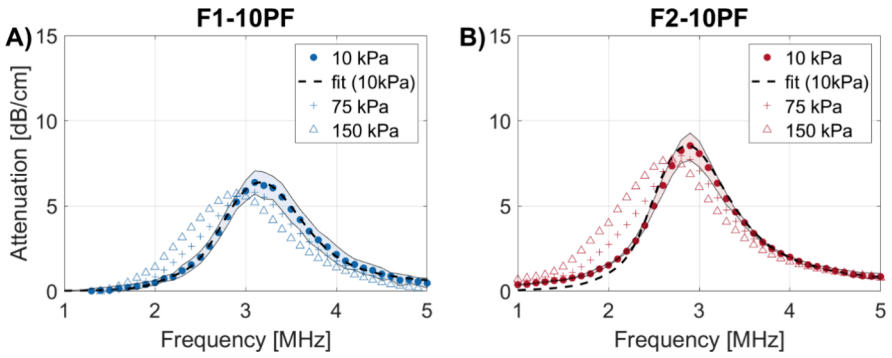

Figure 4. Acoustic attenuation measurements for (A) F1−10PF and (B) F2−10PF microbubbles at acoustic amplitude pressures of 10, 75, and 150 kPa. Transparent shaded region indicates intrameasurement variance at 10 kPa. The fitted curve through the data measured at 10 kPa was used to obtain the shell stiffness and shell viscosity. These measurements were done on the same microbubbles as shown in Figure 2B,E.

Table 1. Size and Shell Properties of Monodisperse Microbubbles at 2 d Postproduction

Formulation	Pluronic F68 (mol %)	R_f (μm)	R_i/R_f	CoV of size distribution (%)	χ (N/m)	κ_s ($\times 10^{-9}$ kg/s)
F1	5	2.16	2.82	11.03	0.83 ± 0.01	2.7 ± 0.9
	7.2	2.05	3.07	11.70	0.78 ± 0.01	1.3 ± 0.7
	10	2.04	3.15	7.27	0.85 ± 0.01	1.6 ± 0.8
F2	5	2.51	2.55	6.33	0.87 ± 0.01	3.4 ± 1.0
	7.2	2.30	2.80	7.13	0.83 ± 0.00	1.9 ± 0.5
	10	2.15	2.98	7.27	0.83 ± 0.00	3.3 ± 1.3

higher flow rates without exceeding the cavitation threshold induced by the Bernoulli pressure drop.[46] Thus, a wider nozzle could alleviate the current bottleneck in achieving higher monodisperse microbubble production rate.[33] In addition, wider nozzles would simplify the microfluidic device fabrication, reduce the likelihood of clogging, and minimize the need for extensive filtration of lipid solution to remove debris.[40]

Attenuation Measurements. Figure 4 displays the attenuation measurements for F1−10PF and F2−10PF microbubble populations 2 d postproduction at acoustic pressures of 10, 75, and 150 kPa, with the transparent shaded region indicating intrameasurement variance at 10 kPa. The peak resonance frequency decreased for higher acoustic pressures because the influence of the microbubble shell decreases for larger radial excursions, and the resonance frequency will shift toward that of a free gas bubble.[37,47] By fitting the data at 10 kPa and leveraging the size distribution from Figure 2Bii,Eii, we derived shell stiffness (χ) values of 0.85 N/m for F1−10PF and 0.83 N/m for F2−10PF, alongside shell viscosities (κs) of 1.6 ± 0.8 × 10^{-9} kg/s for F1−10PF and 3.3 ± 1.3 × 10^{-9} kg/s for F2−10PF.

The shell elasticity χ and shell viscosity κs determined from the acoustic attenuation measurements are summarized in Table 1 for all six studied microbubble populations containing Pluronic F68. The attenuation curves of 5PF and 7.2PF for both formulations are shown in Figure S3. With the same Pluronic F68 addition, F2 microbubble had a higher attenuation than F1. The obtained shell elasticity χ ranged from 0.78 to 0.87 N/m. These shell elasticity values are in line with the 0.5−1.3 N/m range reported for DSPC:DPPE-PEG5000 monodisperse microbubbles, which were obtained from single-microbubble measurements.[23] The lack of a difference between our ternary formulation and their binary formulation suggests that the presence of Pluronic F68 does not influence the shell elasticity. Likewise, no discernible correlation between shell stiffness and additional Pluronic F68 concentration was observed. In terms of shell viscosity, F1 exhibited lower values (average value of 1.9 × 10^{-9} kg/s for 5−10 mol % PF68) in comparison to F2 (average value of 2.9 × 10^{-9} kg/s for 5−10 mol % PF68). Given the substantial variability in the shell viscosity values within the F1 and F2 formulations, namely a factor of 1 for F1 and two for F2, these results are inconclusive regarding the precise impact of Pluronic F68 on shell viscosity.

Repeated Production of F1−10PF and F2−10PF Monodisperse Microbubbles. To assess the repeatability of monodisperse microbubble production, the production process, sizing and acoustical characterization were repeated two times (three in total) using the same formulation. Based on the results so far, the 10PF formulations were selected for further assessments, as for the F1 the 10PF had the highest monodispersity, i.e., the lowest CoV of the size distribution. Although the F2−5PF had a slightly lower CoV out of the F2, F2−10PF was selected to evaluate the influence of PEG40-stearate at the same Pluronic F68 concentration. The size distributions are shown in Figure S4. The mean radius varied per batch, ranging from 1.46 to 2.21 μm due to variations in R_i/R_f. Similarly, the mean microbubble radius remained stable with less than 4% decrease over the 7 d-period for both formulations (Figure S2B). Regarding monodispersity, both F1−10PF and F2−10PF demonstrated an increase in CoV from on-chip to 7 d postproduction (Figure 5), with no clear difference in shelf stability between the two formulations. The attenuation curves of repeated production of both formulations with 10PF addition are shown in Figure S5. The shell elasticity for the repeated F1−10PF showed a slightly higher value of 0.93 N/m, while for F2−10PF this was a slightly lower value of 0.78 N/m (Table 2). Similar to the microbubble batches listed in Table 1, the shell viscosity exhibited variability with no clear pattern for the additional 10PF batches of both formulations.

Dilution Stability. To investigate the stability of microbubbles upon dilution, the size distribution of both F1−10PF and F2−10PF microbubbles diluted in Isotone-II was

https://doi.org/10.1021/acsami.4c18844
ACS Appl. Mater. Interfaces 2025, 17, 8976−8986

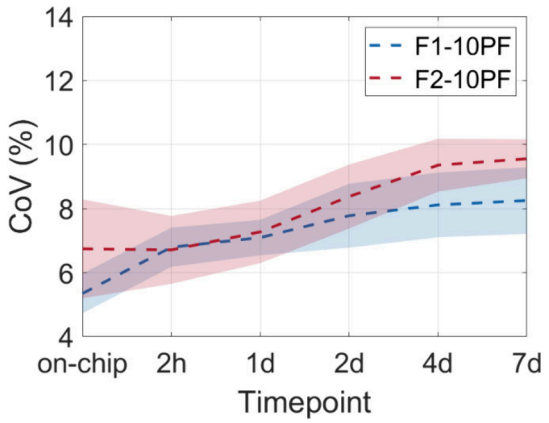

Figure 5. CoV from on-chip to 7 d postproduction for three produced batches of F1−10PF and F2−10PF where the transparent shaded region indicates the standard deviation.

monitored over a 30 min period. The results show a slight decrease in radius for both formulations: F1−10PF exhibited a 3% decrease, while this was around 1.6% for F2−10PF (Figure 6A). The microbubble concentration decreased for both formulations (Figure 6B), with F1−10PF maintaining a lower concentration than F2−10PF during 30 min. Specifically, after 30 min, F1−10PF was at 69% of the starting concentration, compared to 79% for F2−10PF. Despite the decrease in size and concentration over 30 min, monodispersity was maintained for both formulations, with CoV values fluctuating around 7.8% for F1−10PF and around 7.4% for F2−10PF (Figure 6C). Thus, F2−10PF demonstrated better stability upon dilution compared to F1−10PF. Previous studies report mixed effects of PEG40-stearate on the stability of microbubbles, both positive[48] and negative.[49,50] In our study, we compared a binary formulation (F1: DSPC:DPPE-PEG5000) with a ternary formulation (F2: DSPC:DPPE-PEG5000:PEG40-stearate), whereas previous studies[48,49] compared binary formulations where PEG40-stearate was replaced with DSPE-PEG2000. In a ternary mixture, PEG40-stearate may act differently as an emulsifier by promoting lateral phase separation.[51] Another study showed that adding PEG40-stearate to DSPC-based lipid formulations enhances the formation of condensed phases and increases cohesiveness in the lipid shell.[42] The degree of cohesiveness in the lipid shell has, in turn, been linked to critical transport properties, such as gas permeability[52,53] and lipid shedding behavior,[54,55] which are essential for maintaining microbubble stability during dilution and under acoustic excitation. Based on these findings, we speculate that enhanced stability for F2 in comparison to F1 is PEG40-stearate-induced alterations to the microbubble microstructures in F2. Future work is needed to characterize the microstructures in the microbubble shell for these two formulations by using high-resolution microscopy techniques, such as 4Pi confocal microscopy,[34] which could provide more insights into how PEG40-stearate affects the monolayer and its role in stabilizing monodisperse microbubbles. It is important to note that microbubble stability upon intravenous injection is more complex due to factors such as gas exchange, temperature, pressure changes and clearance by the reticuloendothelial system in lung, spleen and liver.[56,57] Further work is needed to compare the *in vivo* stability and circulation half-life of these two formulations.

Subharmonic Measurements. To investigate the ability of the microbubbles to exhibit subharmonics, scattering experiments were performed with a transmit frequency of 3.5 MHz. Figure 7A shows the scattered frequency spectra in response to a driving pulse with a peak negative pressure (PNP) of 350 kPa, for which the three microbubble formulations exhibited subharmonics at 1.75 MHz. The subharmonic scattering amplitude at 1.75 MHz was at least 6 dB higher for the monodisperse microbubbles (F1−10PF in blue, F2−10 PF in red) than for SonoVue (in green), while SonoVue showed a 2 dB higher fundamental amplitude than monodisperse microbubbles at 3.5 MHz. Figure 7B shows the subharmonic-to-fundamental intensity ratio as a function of the driving pressure, which reveals an increase with pressure for all formulations until reaching a plateau. At lower pressure (i.e., PNP < 350 kPa), F1−10PF exhibited a lower subharmonic-to-fundamental intensity ratio compared to F2−10PF and SonoVue. However, the increase in subharmonics was steeper for the monodisperse formulations as pressure increased, with the maximum difference at 350 kPa, where F1−10PF and F2−10PF were 10 dB higher than SonoVue. A strong relation between the excitation frequency and the size of microbubbles that generate subharmonics was previously shown.[58] Therefore, the lower subharmonic content of SonoVue was likely due to the smaller fraction of microbubbles that, owing to the wide size distribution, generated subharmonics. The lower onset threshold, the steeper increase, and the higher subharmonic-to-fundamental ratio of monodisperse microbubbles agree with previous studies comparing the subharmonics of monodisperse and polydisperse microbubbles[17] and suggest potential advantages for noninvasive pressure sensing and improving signal-to-noise ratios.[59] The maximum subharmonic-to-fundamental ratio of our monodisperse microbubbles (−10 dB) was within the range reported in other monodisperse microbubbles studies (from −35 dB to −9 dB).[16,17] However, a direct comparison cannot be established due to the different experimental settings. Further studies are needed to evaluate the performance of these formulations for pressure sensing and compare them with other formulations. It is also worth noting that the subharmonic behavior also

Table 2. Size and Shell Properties of F1-10PF and F2-10PF Microbubbles at 2 d Postproduction[a]

Formulation	R_f (μm)	R_i/R_f	CoV of size distribution (%)	χ (N/m)	κ_s ($\times 10^{-9}$ kg/s)
F1−10PF	2.04	3.15	7.27	0.85 ± 0.01	8.8 ± 0.2
	2.21	2.71	8.93	0.93 ± 0.01	1.4 ± 0.9
	1.81	3.28	7.14		
F2−10PF	2.15	2.98	7.27	0.83 ± 0.00	3.3 ± 1.3
	2.00	2.97	9.13	0.78 ± 0.05	8.4 ± 3.4
	1.46	3.84	8.75		

[a]The top rows of each formulation are the microbubble batch listed in Table 1.

https://doi.org/10.1021/acsami.4c18844
ACS Appl. Mater. Interfaces 2025, 17, 8976−8986

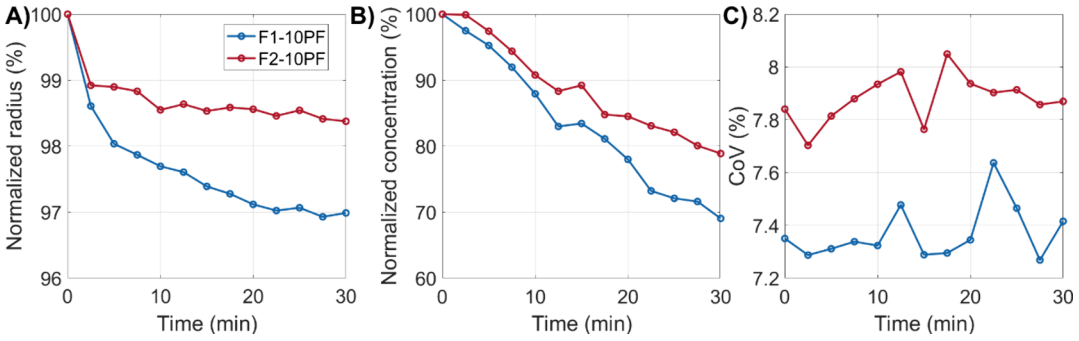

Figure 6. Monodisperse microbubble stability in dilution for F1−10PF and F2−10PF over a 30 min period. (A) Microbubble radius, (B) microbubble concentration, and (C) CoV of the microbubble size distribution.

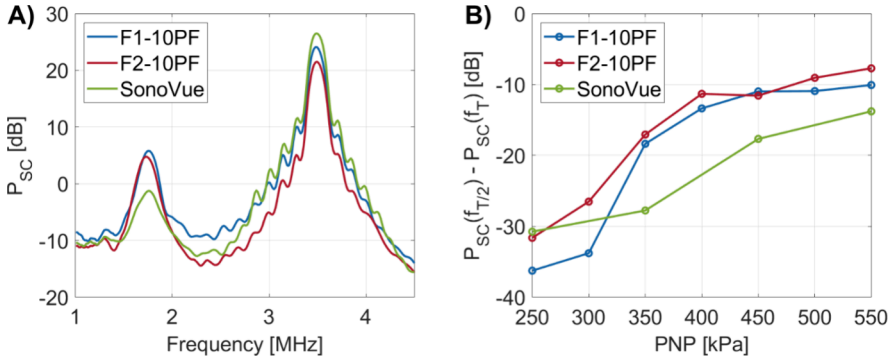

Figure 7. Subharmonic measurements for F1−10PF (blue), F2−10PF (red), and SonoVue (green). (A) Scattering signal measured in response to a 30 cycle, 350 kPa pulse at 3.5 MHz. (B) Ratio of scattered pressure at subharmonic and fundamental frequencies as a function of the driving pressure.

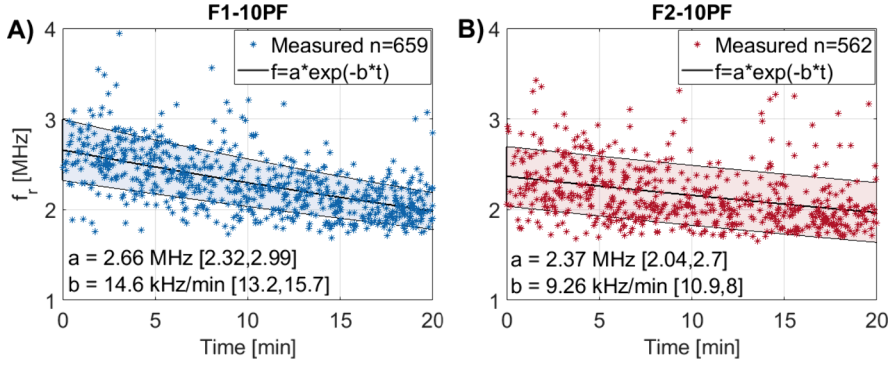

Figure 8. Measured resonance frequencies of individual monodisperse microbubbles in the acoustical camera for (A) F1−10PF and (B) F2−10PF. $f = a \cdot \exp(-b \cdot t)$ was fitted through the $f_{res}(t)$ results to obtain the moving average, as shown by the black line. The standard deviation of the moving average is shown by the transparent region. The displayed values for a and b are the means, and the upper and lower bounds are in between the brackets.

depends on the time in solution,[60] which is outside the scope of this study.

Acoustical Camera Measurements. To investigate the variance in acoustical response of single microbubbles, acoustical camera measurements were conducted for both the F1−10PF and F2−10PF formulations. Figure 8 reveals a spread in resonance frequencies (f_{res}) with a noticeable decrease in frequencies over time in the solution for both formulations. Specifically, for F1−10PF the initial f_{res} of 2.66 MHz decreased by 25.6%, while for F2−10PF the initial f_{res} of 2.37 MHz decreased by 16.9%. The relative spread in the resonance frequencies decreased from 12% to 10% for the F1−10PF microbubbles, while the spread remained a steady 12% for the F2−10PF microbubbles. The observed decreases in resonance frequencies over the 20 min acoustical camera measurement period are unlikely due to ultrasound exposure as a triggering scheme was used to ensure that the low frequency sequences were only transmitted when a microbubble entered the focus. It is therefore more likely that this decrease in resonance frequency is caused by a change in the microbubble size, which is indeed what we observed in the Coulter Counter (Figure 6). Conversely, we found a decrease in the resonance frequency with a decrease in the microbubble size as opposed to an increase in the Minnaert resonance,[61] which can be explained by a loss of shell elasticity[62] as the microbubbles go to a buckled state. This rapid transition to a buckled shell state could also explain the relatively high subharmonic responses, as

https://doi.org/10.1021/acsami.4c18844
ACS Appl. Mater. Interfaces 2025, 17, 8976−8986

buckling is known to promote nonlinear dynamics and thereby lower the threshold for subharmonic generation.[58,63,64]

CONCLUSIONS

Our results suggest that adding 5−10 mol % Pluronic F68 in both a binary and ternary DSPC-based formulation enables the production of stable monodisperse microbubbles using microfluidic flow focusing by effectively suppressing coalescence at room temperature. The produced microbubbles maintained their size and preserved their monodispersity for up to 7 days. The ternary formulation (DPPE-PEG5000 and PEG40-stearate) with 10 mol % Pluronic F68 (i.e., F2−10PF) exhibited better stability in dilution and a smaller decrease in resonance frequency than the binary formulation (DPPE-PEG5000). Additionally, our monodisperse microbubbles had a lower acoustic amplitude threshold for subharmonic generation and stronger subharmonic response than SonoVue. While these findings highlight the potential of the F2−10PF formulation, it is important to note that all experiments were conducted *in vitro*. Further studies are needed to evaluate the behavior of these monodisperse microbubbles in more complex physiological environments. All in all, the ability to produce long-term stable monodisperse microbubbles at room temperature simplifies manufacturing and offers potential for the direct production of drug-loaded or targeted-ready monodisperse microbubbles, enhancing their translational value for clinical applications such as noninvasive pressure sensing, ultrasound molecular imaging, and targeted drug delivery.

ASSOCIATED CONTENT

Supporting Information

The Supporting Information is available free of charge at https://pubs.acs.org/doi/10.1021/acsami.4c18844.

Fabrication method of flow-focusing microfluidic chip; size distributions and acoustic attenuation measurements for microbubbles with 5 and 7.2 mol % Pluronic F68 addition; mean microbubble radius changes for all formulations over a 7 d postproduction period; size distributions and attenuation measurements for repeated production batches of microbubbles with 10 mol % Pluronic F68 addition (PDF)

AUTHOR INFORMATION

Corresponding Author

Yuchen Wang − *Biomedical Engineering, Department of Cardiology, Erasmus MC, Rotterdam 3015 GD, The Netherlands;* orcid.org/0000-0002-3251-0529; Email: y.wang@erasmusmc.nl

Authors

Sander Spiekhout − *Biomedical Engineering, Department of Cardiology, Erasmus MC, Rotterdam 3015 GD, The Netherlands*

Ana Walgode − *Biomedical Engineering, Department of Cardiology, Erasmus MC, Rotterdam 3015 GD, The Netherlands*

Gonzalo Collado-Lara − *Biomedical Engineering, Department of Cardiology, Erasmus MC, Rotterdam 3015 GD, The Netherlands*

Antonius F. W. van der Steen − *Biomedical Engineering, Department of Cardiology, Erasmus MC, Rotterdam 3015 GD, The Netherlands; Department of Imaging Physics, Delft University of Technology, Delft 2628 CJ, The Netherlands*

Nico de Jong − *Biomedical Engineering, Department of Cardiology, Erasmus MC, Rotterdam 3015 GD, The Netherlands; Department of Imaging Physics, Delft University of Technology, Delft 2628 CJ, The Netherlands*

Johannes G. Bosch − *Biomedical Engineering, Department of Cardiology, Erasmus MC, Rotterdam 3015 GD, The Netherlands*

Benjamin R. G. Johnson − *Molecular and Nanoscale Physics Group, School of Physics and Astronomy, University of Leeds, Leeds LS2 9JT, United Kingdom*

Klazina Kooiman − *Biomedical Engineering, Department of Cardiology, Erasmus MC, Rotterdam 3015 GD, The Netherlands;* orcid.org/0000-0002-0607-4989

Complete contact information is available at: https://pubs.acs.org/10.1021/acsami.4c18844

Author Contributions

Yuchen Wang, Conceptualization, Methodology, Investigation, Formal analysis, Writing−original draft. **Sander Spiekhout**, Conceptualization, Methodology, Investigation, Formal analysis, Writing−original draft. **Ana Walgode**, Methodology, Investigation, Formal analysis. **Gonzalo Collado-Lara**, Investigation, Methodology, Writing−original draft. **Antonius F. W. van der Steen**, Supervision, Writing−review and editing. **Nico de Jong**, Investigation, Methodology, Writing−review and editing. **Johannes G. Bosch**, Supervision, Writing−review and editing. **Benjamin R. G. Johnson**, Methodology, Writing−review and editing. **Klazina Kooiman**, Supervision, Conceptualization, Resources, Funding acquisition, Writing−review and editing.

Funding

This work was funded in part by the Applied and Engineering Sciences TTW (VIDI-project 17543; awarded to K.K.), part of NWO, the European Research Council (ERC) under the European Union's Horizon 2020 Research and Innovation Program (Grant Agreement 805308; awarded to K.K.), and project Bubble-X of the research program Ultra-X-Treme (P17-32), which is financed by the Dutch Research Council (NWO).

Notes

The authors declare no competing financial interest.

ACKNOWLEDGMENTS

The authors thank Robert Beurskens from Biomedical Engineering, the Department of Cardiology, and Geert Springeling from the Department of Experimental Medical Instrumentation for technical assistance during the experiments, both from the Erasmus MC, The Netherlands.

REFERENCES

(1) Kooiman, K.; Roovers, S.; Langeveld, S. A. G.; Kleven, R. T.; Dewitte, H.; O'Reilly, M. A.; Escoffre, J. M.; Bouakaz, A.; Verweij, M. D.; Hynynen, K.; Lentacker, I.; Stride, E.; Holland, C. K. Ultrasound-Responsive Cavitation Nuclei for Therapy and Drug Delivery. *Ultrasound Med. Biol.* **2020**, *46*, 1296−1325.

(2) Langeveld, S. A. G.; Meijlink, B.; Kooiman, K. Phospholipid-Coated Targeted Microbubbles for Ultrasound Molecular Imaging and Therapy. *Curr. Opin Chem. Biol.* **2021**, *63*, 171−179.

(3) Greis, C. Ultrasound Contrast Agents as Markers of Vascularity and Microcirculation. *Clinical Hemorheology and Microcirculation* **2009**, *43*, 1−9.

(4) Correas, J. M.; Helenon, O.; Pourcelot, L.; Moreau, J. F. Ultrasound Contrast Agents. Examples of Blood Pool Agents. *Acta Radiol Suppl* **1997**, *412*, 101−112.
(5) Kooiman, K.; Vos, H. J.; Versluis, M.; de Jong, N. Acoustic Behavior of Microbubbles and Implications for Drug Delivery. *Adv. Drug Deliver. Rev.* **2014**, *72C*, 28−48.
(6) Frinking, P.; Segers, T.; Luan, Y.; Tranquart, F. Three Decades of Ultrasound Contrast Agents: A Review of the Past, Present and Future Improvements. *Ultrasound Med. Biol.* **2020**, *46*, 892−908.
(7) de Jong, N.; Emmer, M.; van Wamel, A.; Versluis, M. Ultrasonic Characterization of Ultrasound Contrast Agents. *Med. Biol. Eng. Comput.* **2009**, *47*, 861−73.
(8) Cosgrove, D.; Harvey, C. Clinical Uses of Microbubbles in Diagnosis and Treatment. *Med. Biol. Eng. Comput.* **2009**, *47*, 813−26.
(9) Leighton, T. *The Acoustic Bubble*; Academic Press, 2012.
(10) Schneider, M.; Arditi, M.; Barrau, M. B.; Brochot, J.; Broillet, A.; Ventrone, R.; Yan, F. Br1: A New Ultrasonographic Contrast Agent Based on Sulfur Hexafluoride-Filled Microbubbles. *Invest. Radiol.* **1995**, *30*, 451−7.
(11) Sontum, P. C. Physicochemical Characteristics of Sonazoid, a New Contrast Agent for Ultrasound Imaging. *Ultrasound Med. Biol.* **2008**, *34*, 824−33.
(12) Segers, T.; de Jong, N.; Versluis, M. Uniform Scattering and Attenuation of Acoustically Sorted Ultrasound Contrast Agents: Modeling and Experiments. *J. Acoust Soc. Am.* **2016**, *140*, 2506.
(13) Whittingham, T. A. Contrast-Specific Imaging Techniques: Technical Perspective. In *Contrast Media in Ultrasonography: Basic Principles and Clinical Applications*; Springer, 2005; pp 43−70.
(14) Segers, T.; Kruizinga, P.; Kok, M. P.; Lajoinie, G.; De Jong, N.; Versluis, M. Monodisperse Versus Polydisperse Ultrasound Contrast Agents: Non-Linear Response, Sensitivity, and Deep Tissue Imaging Potential. *Ultrasound in Medicine & Biology* **2018**, *44*, 1482−1492.
(15) van Elburg, B.; Deprez, J.; van den Broek, M.; De Smedt, S. C.; Versluis, M.; Lajoinie, G.; Lentacker, I.; Segers, T. Dependence of Sonoporation Efficiency on Microbubble Size: An in Vitro Monodisperse Microbubble Study. *J. Controlled Release* **2023**, *363*, 747−755.
(16) van Hoeve, W.; de Vargas Serrano, M.; te Winkel, L.; Forsberg, F.; Dave, J. K.; Sarkar, K.; Wessner, C. E.; Eisenbrey, J. R. Improved Sensitivity of Ultrasound-Based Subharmonic Aided Pressure Estimation Using Monodisperse Microbubbles. *J. Ultras Med.* **2022**, *41*, 1781−1789.
(17) Wang, P.; Tan, C.; Ji, X.; Bai, J.; Yu, A. C. H.; Qin, P. Sensitivity Improvement of Subharmonic-Based Pressure Measurement Using Phospholipid-Coated Monodisperse Microbubbles. *Ultrason Sonochem* **2024**, *104*, No. 106830.
(18) Tan, Y.-C.; Cristini, V.; Lee, A. P. Monodispersed Microfluidic Droplet Generation by Shear Focusing Microfluidic Device. *Sens. Actuators, B* **2006**, *114*, 350−356.
(19) Ganan-Calvo, A. M.; Gordillo, J. M. Perfectly Monodisperse Microbubbling by Capillary Flow Focusing. *Phys. Rev. Lett.* **2001**, *87*, No. 274501.
(20) Anna, S. L.; Mayer, H. C. Microscale Tipstreaming in a Microfluidic Flow Focusing Device. *Phys. Fluids* **2006**, *18*, No. 121512.
(21) Segers, T.; De Rond, L.; De Jong, N.; Borden, M.; Versluis, M. Stability of Monodisperse Phospholipid-Coated Microbubbles Formed by Flow-Focusing at High Production Rates. *Langmuir* **2016**, *32*, 3937−3944.
(22) Dhanaliwala, A. H.; Chen, J. L.; Wang, S.; Hossack, J. A. Liquid Flooded Flow-Focusing Microfluidic Device for in Situ Generation of Monodisperse Microbubbles. *Microfluid. Nanofluid.* **2013**, *14*, 457−467.
(23) Spiekhout, S.; van Elburg, B.; Voorneveld, J.; Jong, N. d.; Versluis, M.; Bosch, J. G.; Segers, T. Are Monodisperse Phospholipid-Coated Microbubbles "Mono-Acoustic? *Appl. Phys. Lett.* **2024**, *124*, No. 231601.
(24) Segers, T.; Lohse, D.; Versluis, M.; Frinking, P. Universal Equations for the Coalescence Probability and Long-Term Size Stability of Phospholipid-Coated Monodisperse Microbubbles Formed by Flow Focusing. *Langmuir* **2017**, *33*, 10329−10339.
(25) Segers, T.; Lassus, A.; Bussat, P.; Gaud, E.; Frinking, P. Improved Coalescence Stability of Monodisperse Phospholipid-Coated Microbubbles Formed by Flow-Focusing at Elevated Temperatures. *Lab Chip* **2019**, *19*, 158−167.
(26) Xie, Y.; Dixon, A. J.; Rickel, J. M. R.; Klibanov, A. L.; Hossack, J. A. Closed-Loop Feedback Control of Microbubble Diameter from a Flow-Focusing Microfluidic Device. *Biomicrofluidics* **2020**, *14*, No. 034101.
(27) Rodeheaver, G. T.; Kurtz, L.; Kircher, B. J.; Edlich, R. F. Pluronic F-68: A Promising New Skin Wound Cleanser. *Ann. Emerg Med.* **1980**, *9*, 572−6.
(28) Moloughney, J. G.; Weisleder, N. Poloxamer 188 (P188) as a Membrane Resealing Reagent in Biomedical Applications. *Recent Patents on Biotechnology* **2012**, *6*, 200−211.
(29) Chen, Z.; Chattaraj, R.; Pulsipher, K. W.; Karmacharya, M. B.; Hammer, D. A.; Lee, D.; Sehgal, C. M. Photoacoustic and Ultrasound Dual-Mode Imaging Via Functionalization of Recombinant Protein-Stabilized Microbubbles with Methylene Blue. *ACS Appl. Bio Mater.* **2019**, *2*, 4020−4026.
(30) Angile, F. E.; Vargo, K. B.; Sehgal, C. M.; Hammer, D. A.; Lee, D. Recombinant Protein-Stabilized Monodisperse Microbubbles with Tunable Size Using a Valve-Based Microfluidic Device. *Langmuir* **2014**, *30*, 12610−8.
(31) Chen, Z.; Pulsipher, K. W.; Chattaraj, R.; Hammer, D. A.; Sehgal, C. M.; Lee, D. Engineering the Echogenic Properties of Microfluidic Microbubbles Using Mixtures of Recombinant Protein and Amphiphilic Copolymers. *Langmuir* **2019**, *35*, 10079−10086.
(32) Shih, R.; Bardin, D.; Martz, T. D.; Sheeran, P. S.; Dayton, P. A.; Lee, A. P. Flow-Focusing Regimes for Accelerated Production of Monodisperse Drug-Loadable Microbubbles toward Clinical-Scale Applications. *Lab Chip* **2013**, *13*, 4816.
(33) Segers, T.; Gaud, E.; Casqueiro, G.; Lassus, A.; Versluis, M.; Frinking, P. Foam-Free Monodisperse Lipid-Coated Ultrasound Contrast Agent Synthesis by Flow-Focusing through Multi-Gas-Component Microbubble Stabilization. *Appl. Phys. Lett.* **2020**, *116*, No. 173701.
(34) Langeveld, S. A. G.; Beekers, I.; Collado-Lara, G.; van der Steen, A. F. W.; de Jong, N.; Kooiman, K. The Impact of Lipid Handling and Phase Distribution on the Acoustic Behavior of Microbubbles. *Pharmaceutics* **2021**, *13*, 119.
(35) Jang, Y.; Jang, W. S.; Gao, C.; Shim, T. S.; Crocker, J. C.; Hammer, D. A.; Lee, D. Tuning the Mechanical Properties of Recombinant Protein-Stabilized Gas Bubbles Using Triblock Copolymers. *ACS Macro Lett.* **2016**, *5*, 371−376.
(36) Abou-Saleh, R. H.; Armistead, F. J.; Batchelor, D. V. B.; Johnson, B. R. G.; Peyman, S. A.; Evans, S. D. Horizon: Microfluidic Platform for the Production of Therapeutic Microbubbles and Nanobubbles. *Rev. Sci. Instrum.* **2021**, *92*, No. 074105.
(37) Segers, T.; Gaud, E.; Versluis, M.; Frinking, P. High-Precision Acoustic Measurements of the Nonlinear Dilatational Elasticity of Phospholipid Coated Monodisperse Microbubbles. *Soft Matter* **2018**, *14*, 9550−9561.
(38) Renaud, G.; Bosch, J. G.; Van Der Steen, A. F. W.; De Jong, N. Low-Amplitude Non-Linear Volume Vibrations of Single Microbubbles Measured with an "Acoustical Camera". *Ultrasound in Medicine and Biology* **2014**, *40*, 1282−1295.
(39) Talu, E.; Hettiarachchi, K.; Powell, R. L.; Lee, A. P.; Dayton, P. A.; Longo, M. L. Maintaining Monodispersity in a Microbubble Population Formed by Flow-Focusing. *Langmuir* **2008**, *24*, 1745−1749.
(40) Shih, R.; Lee, A. P. Post-Formation Shrinkage and Stabilization of Microfluidic Bubbles in Lipid Solution. *Langmuir* **2016**, *32*, 1939−1946.
(41) Langeveld, S. A. G.; Schwieger, C.; Beekers, I.; Blaffert, J.; van Rooij, T.; Blume, A.; Kooiman, K. Ligand Distribution and Lipid Phase Behavior in Phospholipid-Coated Microbubbles and Monolayers. *Langmuir* **2020**, *36*, 3221−3233.

https://doi.org/10.1021/acsami.4c18844
ACS Appl. Mater. Interfaces 2025, 17, 8976−8986

(42) Borden, M. A.; Pu, G.; Runner, G. J.; Longo, M. L. Surface Phase Behavior and Microstructure of Lipid/Peg-Emulsifier Monolayer-Coated Microbubbles. *Colloids Surf. B Biointerfaces* **2004**, *35*, 209−23.
(43) Soysal, U.; Azevedo, P. N.; Bureau, F.; Aubry, A.; Carvalho, M. S.; Pessoa, A. C. S. N.; Torre, L. G. D. l.; Couture, O.; Tourin, A.; Fink, M.; Tabeling, P. Freeze-Dried Microfluidic Monodisperse Microbubbles as a New Generation of Ultrasound Contrast Agents. *Ultrasound Med. Biol.* **2022**, *48*, 1484−1495.
(44) Frey, S. L.; Lee, K. Y. C. Temperature Dependence of Poloxamer Insertion into and Squeeze-out from Lipid Monolayers. *Langmuir* **2007**, *23*, 2631−2637.
(45) Maskarinec, S. A.; Hannig, J.; Lee, R. C.; Lee, K. Y. C. Direct Observation of Poloxamer 188 Insertion into Lipid Monolayers. *Biophys. J.* **2002**, *82*, 1453−1459.
(46) Cleve, S.; Lassus, A.; Diddens, C.; van Elburg, B.; Gaud, E.; Cherkaoui, S.; Versluis, M.; Segers, T.; Lajoinie, G. Microbubble Formation by Flow Focusing: Role of Gas and Liquid Properties, and Channel Geometry. *J. Fluid Mech.* **2023**, *972*, No. A27.
(47) Wu, J.; Nyborg, W. L. Ultrasound, Cavitation Bubbles and Their Interaction with Cells. *Adv. Drug Deliv Rev.* **2008**, *60*, 1103−16.
(48) Kwan, J. J.; Borden, M. A. Lipid Monolayer Collapse and Microbubble Stability. *Adv. Colloid Interface Sci.* **2012**, *183*−*184*, 82−99.
(49) Owen, J.; Kamila, S.; Shrivastava, S.; Carugo, D.; Bernardino De La Serna, J.; Mannaris, C.; Pereno, V.; Browning, R.; Beguin, E.; Mchale, A. P.; Callan, J. F.; Stride, E. The Role of Peg-40-Stearate in the Production, Morphology, and Stability of Microbubbles. *Langmuir* **2019**, *35*, 10014−10024.
(50) Lozano, M. M.; Longo, M. L. Microbubbles Coated with Disaturated Lipids and Dspe-Peg2000: Phase Behavior, Collapse Transitions, and Permeability. *Langmuir* **2009**, *25*, 3705−12.
(51) Borden, M. A.; Martinez, G. V.; Ricker, J.; Tsvetkova, N.; Longo, M.; Gillies, R. J.; Dayton, P. A.; Ferrara, K. W. Lateral Phase Separation in Lipid-Coated Microbubbles. *Langmuir* **2006**, *22*, 4291−7.
(52) Borden, M. Nanostructural Features on Stable Microbubbles. *Soft Matter* **2009**, *5*, 716−720.
(53) Pu, G.; Longo, M. L.; Borden, M. A. Effect of Microstructure on Molecular Oxygen Permeation through Condensed Phospholipid Monolayers. *J. Am. Chem. Soc.* **2005**, *127*, 6524−6525.
(54) Borden, M. A.; Dayton, P.; Zhao, S. K.; Ferrara, K. W. Physico-Chemical Properties of the Microbubble Lipid Shell - Composition, Microstructure & Properties of Targeted Ultrasound Contrast Agents. *2004 IEEE Ultrasonics Symposium* **2004**, *1*, 20−23.
(55) Borden, M. A.; Kruse, D. E.; Caskey, C. F.; Zhao, S. K.; Dayton, P. A.; Ferrara, K. W. Influence of Lipid Shell Physicochemical Properties on Ultrasound-Induced Microbubble Destruction. *Ieee T Ultrason Ferr* **2005**, *52*, 1992−2002.
(56) Garg, S.; Thomas, A. A.; Borden, M. A. The Effect of Lipid Monolayer in-Plane Rigidity on in Vivo Microbubble Circulation Persistence. *Biomaterials* **2013**, *34*, 6862−70.
(57) Morel, D. R.; Schwieger, I.; Hohn, L.; Terrettaz, J.; Llull, J. B.; Cornioley, Y. A.; Schneider, M. Human Pharmacokinetics and Safety Evaluation of Sonovue, a New Contrast Agent for Ultrasound Imaging. *Invest Radiol* **2000**, *35*, 80−5.
(58) Sijl, J.; Dollet, B.; Overvelde, M.; Garbin, V.; Rozendal, T.; de Jong, N.; Lohse, D.; Versluis, M. Subharmonic Behavior of Phospholipid-Coated Ultrasound Contrast Agent Microbubbles. *J. Acoust Soc. Am.* **2010**, *128*, 3239−52.
(59) Forsberg, F. Subharmonic-Aided Pressure Estimation (Shape): On the Cusp of Clinical Utility? *Eur. Radiol* **2024**, *34*, 755−757.
(60) Kanbar, E.; Fouan, D.; Sennoga, C. A.; Doinikov, A. A.; Bouakaz, A. Impact of Filling Gas on Subharmonic Emissions of Phospholipid Ultrasound Contrast Agents. *Ultrasound Med. Biol.* **2017**, *43*, 1004−1015.
(61) Minnaert, M. Xvi. On Musical Air-Bubbles and the Sounds of Running Water. *London, Edinburgh, and Dublin Philosophical Magazine and Journal of Science* **1933**, *16*, 235−248.
(62) Marmottant, P.; Van Der Meer, S.; Emmer, M.; Versluis, M.; De Jong, N.; Hilgenfeldt, S.; Lohse, D. A Model for Large Amplitude Oscillations of Coated Bubbles Accounting for Buckling and Rupture. *J. Acoust. Soc. Am.* **2005**, *118*, 3499−3505.
(63) Sijl, J.; Overvelde, M.; Dollet, B.; Garbin, V.; de Jong, N.; Lohse, D.; Versluis, M. Compression-Only″ Behavior: A Second-Order Nonlinear Response of Ultrasound Contrast Agent Microbubbles. *J. Acoust Soc. Am.* **2011**, *129*, 1729−39.
(64) Prosperetti, A. A General Derivation of the Subharmonic Threshold for Non-Linear Bubble Oscillations. *J. Acoust Soc. Am.* **2013**, *133*, 3719−26.

https://doi.org/10.1021/acsami.4c18844
ACS Appl. Mater. Interfaces 2025, 17, 8976−8986